Constraints on global oceanic emissions of N_2O from observations and models

Erik T. Buitenhuis[1,2], Parvadha Suntharalingam[1], and Corinne Le Quéré[1,2]

[1]School of Environmental Sciences, University of East Anglia, Norwich, United Kingdom
[2]Tyndall Centre for Climate Change Research, University of East Anglia, Norwich, United Kingdom

Correspondence to: Erik T. Buitenhuis (E-mail: http://greenocean-data.uea.ac.uk/.feedback.html)

Abstract. We estimate the global ocean N_2O flux to the atmosphere and its confidence interval using a statistical method based on model perturbation simulations and their fit to a database of ΔpN_2O (n=6136). We evaluate two submodels of N_2O production. The first submodel splits N_2O production into oxic and hypoxic pathways following previous publications. The second submodel explicitly represents the redox transformations of N that lead to N_2O production (nitrification and hypoxic denitrification) and N_2O consumption (suboxic denitrification), and is presented here for the first time. We perturb both submodels by modifying the key parameters of the N_2O cycling pathways (nitrification rates, NH_4^+ uptake, N_2O yields under oxic, hypoxic and suboxic conditions), and determine a set of optimal model parameters by minimisation of a cost function against 4 databases of N cycle observations derived from observed and model ΔpN_2O concentrations. Our estimate of the global oceanic N_2O flux resulting from this cost function minimisation is 2.4 ± 0.8 and 2.5 ± 0.8 Tg N y^{-1} for the 2 N_2O submodels. These estimates suggest that the currently available observational data of surface ΔpN_2O constrain the global N_2O flux to a narrower range relative to the large range of results presented in the latest IPCC report.

1 Introduction

Nitrous oxide (N_2O) is the third most important contributor to anthropogenic radiative forcing, after carbon dioxide (CO_2) and methane (CH_4) (Myhre et al., 2013). It is also currently estimated as the dominant contributor to stratospheric ozone depletion (Portmann et al., 2012). Yet our quantitative understanding of the magnitude and processes controlling natural N_2O emissions from the Earth surface to the atmosphere is very poor. A range of methods have been used to constrain total oceanic N_2O emissions, including the combination of surface ocean N_2O partial pressure anomalies with gas-exchange parameterizations (Nevison et al., 1995), empirically derived functional relationships applied to global ocean datasets (Nevison et al., 2003; Freing et al., 2012), and ocean biogeochemistry models (Suntharalingam and Sarmiento, 2000; Suntharalingam et al., 2000; Jin and Gruber, 2003; Martinez-Rey et al., 2015). In spite of the multiple methods used, the reported oceanic emissions of N_2O is still poorly constrained, ranging from 1.9 to 9.4 Tg N y^{-1} according to the latest report of the Intergovernmental Panel on Climate Change (IPCC Ciais et al., 2013). The uncertainty in the oceanic emissions of N_2O accounts for a large part of the total uncertainty in the natural N_2O emissions, which are approximately 11 Tg N y^{-1} (Ciais et al., 2013). Part of the uncertainty in the oceanic emissions is whether estuaries are included, which could emit as much as 2.3 - 3.6 Tg N y^{-1} (Bange et al., 1996).

The large uncertainty in the oceanic emissions of N_2O stems from the complexity of its production pathways. There are two main pathways of N_2O production in the ocean, nitrification and denitrification, which both stem from redox reactions of nitrogen, under oxic and hypoxic conditions, respectively (Fig. 1). N_2O is formed as a byproduct of marine nitrification of ammonium (NH_4^+) to nitrate (NO_3^-); N_2O is also an intermediate product of denitrification, during the reduction of NO_3^- to nitrogen gas (N_2) (Frame and Casciotti, 2010; Loescher et al., 2012; Merbt et al., 2012). Denitrification can also consume N_2O, using extracellular N_2O, and reduce it to N_2 (Bange, 2008). In the oxic part of the ocean (i.e. most of the ocean, 97% >34 μmol O_2 L^{-1} (using O_2 data taken from Bianchi et al., 2012)) denitrification is suppressed, and the primary formation pathway is usually ascribed to nitrification (Cohen and Gordon, 1978), although denitrification may be significant in the anaerobic centres of large marine snow particles in oxic waters (Klawonn et al., 2015). Oceanic N_2O production in oxic regions is often derived from the linear relationships observed between apparent oxygen utilization (AOU) and apparent N_2O production (ΔN_2O) (e.g. Yoshinari, 1976; Cohen and Gordon, 1978). However, the ΔN_2O/AOU ratio varies in different water masses and oceanic regions (Suntharalingam and Sarmiento, 2000). Previous studies have suggested that differences in the ΔN_2O/AOU ratio could be driven by changing N_2O yields under varying pressure and temperature (Butler et al., 1989) or varying O_2 concentration (Nevison et al., 2003). Additional mechanisms not yet quantified could include variations in the elemental stoichiometry of the organic matter that is being remineralised, and spatial separation of organic matter remineralisation and nitrification. Throughout the manuscript we will refer to N_2O stoichiometries relative to O_2, NH_4^+ and NO_3^- as ratios, because they have been optimised against global databases of concentration measurements, rather than from microbiological yields. Using the latter would be more mechanistically satisfying, but the relevant yields are at present insufficiently constrained by observations.

Estimates of the contribution from suboxic regions of the ocean (about 3%) to the global N_2O flux vary from net depletion via denitrification (Cohen and Gordon, 1978), to 33% for the total N_2O production in the suboxic ocean (Suntharalingam et al., 2012), and to more than 50% from denitrification alone (Yoshida et al., 1989). This ambiguity remains unresolved. Bottom-up microbial physiology data is relatively scarce (see Sect. 2.4 - 2.6), while top-down data needs relatively complicated inverse methods to estimate the contribution from suboxic regions. These inverse methods are complicated both because of the variation in the ΔN_2O/AOU ratio, which is negative under suboxic conditions, maximal under hypoxic conditions and lower under oxic conditions (e.g. 0.31 - 0.033 mmol/mol, Law and Owens, 1990), and because the influence of mixing gradients make in situ ratios an unreliable gauge to the biological yields under in situ conditions (Nevison et al., 2003).

Here, we estimate the global ocean N_2O flux to the atmosphere and its confidence interval. First, we estimate N_2O flux from observations only (Sect. 2.1). This estimate has large uncertainty. We subsequently use a statistical approach introduced by Buitenhuis et al. (2013a) to estimate the global oceanic emissions of N_2O and its confidence interval by combining ocean N_2O model simulations with a global database of measurements of surface ΔpN_2O. This approach involves minimisation of a cost function that compares a series of model simulations with a global database of point measurements of surface ΔpN_2O. To achieve this, we use 4 observational databases of the N cycle (Sect. 2.2) to extend the global ocean biogeochemistry model PlankTOM10 (Le Quere et al., 2016b) with additional N cycle processes. We derive the biogeochemical parameters for nitrification rate and phytoplankton use of NH_4^+ from the observational databases of nitrification rate and NH_4^+ concentration (databases (1) and (2) and Sect. 2.4-2.5). Then, we describe two separate submodels of different levels of complexity that represent N_2O cycling pathways (Sect. 2.6-2.7). Finally, we apply the statistical approach (Sect. 2.8) to the two submodels to estimate the N_2O production in the low O_2 regions from the depth resolved N_2O concentration database (database (3) and Sect. 3.1), and the global oceanic N_2O flux from the surface ΔpN_2O database (database (4) and Sect. 3.2), followed by a discussion of the results (Sect. 4).

2 Ocean N cycle

2.1 Calculation of global ocean N_2O production from N cycle observations

In this section we provide an initial estimate of global marine N_2O production based on observationally derived quantities characterising marine productivity and the global ocean N cycle. This follows a similar method to Cohen and Gordon (1979), who estimated ocean N_2O production using Redfield type ratios. N_2O is produced either during production of NO_3^- in NH_4^+oxidation or during NO_3^- reduction in denitrification (Fig. 1). We therefore base the N_2O production on total NO_3^- turnover, calculated from primary production times the f-ratio. The f-ratio is the fraction of primary production that is supported by nitrate. Primary production (PP) was estimated at 58 ± 7 Pg C y^{-1} based on ^{14}C primary production measurements (n=50,050), parameter perturbations of a previous version of the model used here, and Eq. 5 (Buitenhuis et al., 2013a). We compiled a database of uptake rates of NO_3^-, NH_4^+ and urea, which gives an average f-ratio of 0.29 ± 0.18 (Fig. 2, large symbols, n=34). The globally averaged ΔN_2O/AOU ratio was calculated from the MEMENTO database (Bange et al., 2009) as 81.5 ± 1.4 μmol/mol (Fig. 3). Finally, since primary production is expressed in carbon terms, and N_2O production was correlated with oxygen (O_2) utilization, we need to include the -O_2:C ratio (the - sign indicates the O_2 is consumed as CO_2 is produced), which was taken from Anderson and Sarmiento (1994) as 170 ± 10 / 117 ± 14, and the molar weights of C (12) and N in N_2O (28). Here and in the rest of the paper, errors were progagated in the usual way:

$$error = \sqrt{(\frac{errorofA}{A})^2 + (\frac{errorofB}{B})^2 + ...} * A * B * ... \tag{1}$$

Thus N_2O production was calculated as PP *f-ratio*-O_2:C *ΔN_2O/AOU. Our best estimate of N_2O production using this method is 58 ± 7 *1000 *0.29 ± 0.18 *170 ± 10 /117 ± 14 *81.5e-6 ± 1.4e-6 *28 /12 = 4.6 ± 3.1 Tg N y^{-1}. This estimate lies in the middle of other reported estimates (Fig. 4) but the 68% confidence interval is very large. We therefore investigate the N_2O fluxes using a model optimised with observations in the rest of the paper.

2.2 Observational databases for model development

We used four databases to tune or optimise different aspects of the N cycle in the PlankTOM10 ocean biogeochemistry model. The number of datapoints reported for each database are after gridding to 1°× 1°× 12 months × 33 depths (World Ocean Atlas 2009). The databases used are (1) NH_4^+ specific nitrification rate (d^{-1}, raw data n=425, gridded data n=296) as described in Yool et al. (2007); (2) surface NH_4^+ concentration distribution (μmol L^{-1}, raw data n=33079, gridded data n=2343) that combines the dataset used in Paulot et al. (2015) with data held by the British Oceanographic Data Centre in January 2014

(Johnson et al. in prep., http://www.bodc.ac.uk); (3) depth-resolved N_2O concentration from the MEMENTO project (nmol L^{-1}, https://memento.geomar.de/; Bange et al., 2009, ; downloaded 4 June 2014, raw data n=14342, gridded data n=8047); and (4) surface partial pressure of N_2O (pN_2O) also from MEMENTO (ppb, downloaded 16 Sept. 2015, raw data n=227463, gridded data n=6136). Since there is at present no formal quality control beyond that performed by individual contributors to the MEMENTO database and a check by the database administrators that the values make physical sense (Kock and Bange, 2015), we have taken the database at face value. pN_2O was converted to ΔpN_2O using atmospheric pN_2O:

$$pN_2O_{atm} = 0.000009471353 \times Y^3 - 0.052147139 \times Y^2 + 95.68066 \times Y - 58228.41 \tag{2}$$

(A. Freing, pers. comm., correction to Freing et al., 2009), in which Y is the decimal year. The average absolute difference relative to the global average pN_2O_{atm} data from the NOAA/ESRL Global Monitoring Division (ftp://ftp.cmdl.noaa.gov/hats/n2o/combined/HATS_global_N2O.txt) is 0.5 ppb between 1977 and 2014 and 0.3 ppb between 2000 and 2014.

2.3 Cost Function Formulation

To parameterise the model N cycle, we use a cost function to minimize the difference between model and observations, following the methods of Buitenhuis et al. (2013a):

$$costfunction = 10^{\Sigma|log_{10}(model/observation)|/n} \tag{3}$$

This formulation gives equal weight to the relative correspondence between model and observations at small and large observational values. A value of 2 means that, on average, the model deviates from the observations by a factor 2 in either direction. To calculate the cost function (and also to calculate MSE in Eq. 6), the model was regridded to the same grid as the observations, and residuals were calculated at months and places where there are observations. The cost function results for the optimised simulations are summarised in Table 1.

2.4 Nitrification

Our initial biogeochemical model configuration is PlankTOM10 (Le Quere et al., 2016b), which represents growth and loss terms from ten Plankton Functional Types (PFTs), including N_2-fixers, picoheterotrophs (*Bacteria* plus *Archaea*) and denitrification rate, but not denitrifier biomass. A full model description and parameter values are provided in the supplementary material. Here, we extend the model representation of redox reactions in the N cycle, to create the global biogeochemical model PlankTOM10.2. We describe the new N cycle components below.

In order to represent nitrification rate, the state variable for dissolved inorganic nitrogen was split into NO_3^- and NH_4^+. Respiration by all PFTs produces NH_4^+. The parameterization for nitrification used in our model is based on the analysis of a database of NH_4^+-specific nitrification rates (Yool et al., 2007). Yool et al. (2007) found that observed nitrification rates are highly variable, with no obvious relationship with either latitude or depth. In their model they therefore used a constant rate of 0.2 d^{-1} throughout the ocean. Implementing this rate in our model resulted in a cost function relative to the nitrification rate observations of 4.22 (Table 1). We tested if including temperature, O_2 or light dependence improves the ability of the model to reproduce observed nitrification rates. Regarding the response of ammonia oxidizing *Archaea* (AOA), the main nitrifiers in the ocean (Francis et al., 2005; Wuchter et al., 2006; Loescher et al., 2012), to temperature, we are only aware of the measurements of Qin et al. (2014). These show a ~4-fold variation in maximum growth rate between 3 strains, which poorly constrains the temperature dependence of AOA. We therefore first used a generic Q_{10} of 2 and optimised the rate at 0°C using the nitrification rate observations. This led to only a slightly improved representation of the observations (cost function = 4.18). Although the response of AOA and ammonia oxidizing *Bacteria* (AOB) to O_2 has only been measured at 21-25 °C (Frame and Casciotti, 2010; Loescher et al., 2012), which limits the range of O_2 concentrations, there was a significant logarithmic relationship between N_2O yield and O_2 (Fig. 5). A logarithmic function fit the data better than linear, exponential or power functions. Since nitrification consumes O_2, in the model it decreases as remineralisation switches from O_2 to NO_3 (supplementary material Eq. 70, 61, 67). Implementing this response to O_2 led to only a further small improvement of the model nitrification rate relative to the observations (cost=4.16). This implies that nitrification never becomes O_2 limited, reflecting a lack of data to parameterise an expected decrease. As will be described more fully in Sect. 3.1, we used observed O_2 concentrations in the simulations (Bianchi et al., 2012) rather than interactively modelled O_2, to minimise the impact of model biases in simulated O_2 fields (Suntharalingam et al., 2012). The response of AOA to light is estimated to be 50% inhibited at 5 μmol photons m^{-2} s^{-1}. However, this estimate is not well constrained (Merbt et al., 2012). Implementing this light response did not improve the model, either in combination with the O_2 and temperature responses or with the temperature response only, and was subsequently omitted. The lack of improvement in nitrification rates by adding light inhibition might reflect the lower sensitivity of AOA to light found by Qin et al. (2014).

2.5 Phytoplankton $K_{1/2}$ for NH_4^+ uptake

We used the calculation of the preferential uptake of NH_4^+ over NO_3^- by phytoplankton PFTs of Vallina and Le Quere (2008)(supplementary material Eq. 9). The $K_{1/2}$ of phytoplankton for NH_4^+ has mostly been measured based on uptake rates (syntheses by Goldman and PM, 1983; Killberg-Thoreson et al., 2014). Aksnes and Egge (1991) have shown a theoretical expectation of a linear increase of $K_{1/2}$ with cell radius. The observations are so variable that they neither confirm nor contradict such an increase. The model uses a fixed C:N:O_2 ratio for all organic matter of 122:16:-172, and Michaelis-Menten kinetics for growth based on inorganic N uptake by phytoplankton (Buitenhuis et al., 2013a, supplementary material Eq. 8, 9). We therefore need a $K_{1/2}$ for growth rather than for uptake to be consistent with the fixed C:N ratio (Morel, 1987). The available uptake rate data do not include the supporting data to allow conversion to the $K_{1/2}$ for growth. We are only aware of measurements of the $K_{1/2}$ for growth by Stawiarski (2014). Based on the latter values of 0.09 ± 0.15 μmol L^{-1} for picoeukaryotes, the $K_{1/2}$ of phytoplankton for NH_4^+ was set to 0.1 to 5 μmol L^{-1}, increasing linearly with nominal size (Buitenhuis et al., 2013b). Due to the highly dynamic nature of NH_4^+ turnover, the model produces a much smoother distribution of NH_4^+ concentrations than the observations, but the large scale pattern of surface NH_4^+ concentration shows an increase with latitude, consistent with the observations (Fig. 6), which translates into a cost function of 3.0.

2.6 N_2O production

N_2O production is implemented as two distinct submodels. The diagnostic submodel is based on statistical relationships of ΔN_2O/AOU ratios taken from observations and has previously been published (Suntharalingam et al., 2000, 2012). In oxic waters it uses one ratio to estimate the open ocean source of N_2O production. In hypoxic waters it uses a higher ratio to represent the increased yield of N_2O from both nitrification and denitrification in oxygen minimum zones. The hypoxic N_2O yield is maximal at 1 μmol O_2 L^{-1}, and decreases with an e-folding concentration of 10 μmol O_2 L^{-1} (Suntharalingam et al., 2000, 2012, supplementary material Eq. 69, 35, 67). Previous studies using regional databases have found different oxic ratios (Suntharalingam and Sarmiento, 2000, and references therein). Therefore, both the oxic and hypoxic ratios have been reoptimised to the global databases (Sect. 3.1 - 3.2).

The prognostic submodel presented here is based on process understanding and explicitly represents the primary N_2O formation and consumption pathways associated with the marine nitrogen cycle (Fig. 1). It includes the production of N_2O during oxic nitrification (blue arrows in Fig. 1) and during hypoxic denitrification (red arrow in Fig. 1); and a consumption term during denitrification at even lower (suboxic) O_2 concentrations (yellow arrow in Fig. 1). The ratios of the three processes are globally invariant (supplementary material Eq. 70, 61, 63, 71). The functional form of the O_2 dependence of N_2O consumption (suppl. Eq. 71) was the same as that of denitrification (suppl. Eq. 67), and with an O_2 response function that is 1.5 μmol L^{-1} lower than that of denitrification, which is similar to that used by Babbin et al. (2015). We independently optimised the ratios of N2O production and consumption from denitrification (Sect. 3.1), which controls the net N2O production as a function of O_2 concentration. There is not enough information at present to optimise the O_2 concentration parameters of denitrification and N_2O consumption as well. The low O_2 ratios of both submodels (supplementary material Section 8.7) were optimised using the database of observed N_2O concentration (Sect. 3.1) and the oxic ratios of both submodels were optimised using the database of observed ΔpN_2O (Sect. 3.2). The N2O concentrations from both the diagnostic and the prognostic submodels are transported in the same way by physical transport and the formulation of their gas exchange is also identical.

2.7 N_2O flux and simulation setup

N_2O is transported like other tracers. N_2O flux (=air-sea gas exchange) is calculated as:

$$N_2Oflux = (pN_2O_{atm} * K0 * (1 - p_{watervapor}) - pN_2O) * piston\_velocity * \sqrt{660/Schmidt\_number_{N_2O}} * (1 - ice\_cover) \tag{4}$$

, in which K0 is the solubility (Weiss and Price, 1980), $p_{watervapor}$ is the water vapor pressure (Sarmiento et al., 1992), piston velocity = 0.27*(wind speed)^2 (Sweeney et al., 2007), which is optimised for use with the NCEP reanalysis data used here, the Schmidt number for N_2O was taken from Wanninkhof (1992), and the ice cover is calculated by the sea ice model LIM2.

In most of the simulations, atmospheric pN_2O was calculated from Eq. 2. For the optimised low O_2 production we also ran a series of simulations with the NOAA pN_2O_{atm} observational data that included seasonal and latitudinal variations (see Sect. 2.2 for the ftp address where we downloaded the data, and Sect. 3.2 for the results). Between 2000 and 2014, we used the monthly observations for the 12 available latitudes. Monthly anomalies relative to the global average were calculated at each available latitude from the 2000-2016 observations. These were added to Eq. 2 from 1965 and 1976, and to the global average observations between 1977 and 1999. In the model simulation, the data were linearly interpolated between the 12 latitudes and monthly observations.

The PlankTOM10.2 biogeochemical model coupled with the two N_2O submodels is incorporated into the ocean general circulation model NEMO v3.1 (Madec, 2008). The model resolution is 2° in longitude, on average 1.1° in latitude and has 30 vertical layers, from 10 m in the top 100 m to 500 m at 5000 m. The model simulations were initialised in 1965 from observations (Le Quere et al., 2016b), with NH_4^+ initialised as 0, and N_2O initialised from a horizontal interpolation of the MEMENTO observations (see Sect. 2.2). Simulations were run to 2014, forced with daily atmospheric conditions from the NCEP reanalysis (Kalnay et al., 1996), (for details see Buitenhuis et al., 2013a). Results are reported averaged over the last 5 years.

2.8 Estimation of global N_2O flux from point measurements of ΔpN_2O

In previous versions of the PlankTOM model (Buitenhuis et al., 2006, 2010, 2013a) we have used Eq. 3 to evaluate the model because it minimises relative error, which we have found to be more appropriate when the observations span several orders of magnitude. Unfortunately, statistical confidence intervals have only been defined for χ^2-statistics such as Eq. 5 and 6, which minimise absolute error, so that we end up with 2 cost functions (Eq. 3, 5), depending on the application. To estimate the global air-sea flux of N_2O that best fits the ΔpN_2O data, and its ±1-sigma (68%) confidence interval, we use the formula described in Buitenhuis et al. (2013a):

$$MSE/MSE_{min} = 0.468 \times n/(n-2) \times \sqrt{(2(2n-2)/(n(n-4))) + n/(n-2)} \tag{5}$$

, in which MSE is mean square error:

$$MSE = \frac{\Sigma(model(longitude, latitude, month) - observation(longitude, latitude, month))^2}{n} \tag{6}$$

, MSE_{min} is the MSE of the model simulation that is closest to the observations, and n is the number of gridded observations.

In addition to the uncertainty that arises from the model-observations mismatch, uncertainty is contributed by the uncertainties in the N_2O solubility and the piston velocity, the two quantities that connect the measured ΔpN_2O to the estimated air-sea flux. The uncertainty in the solubility has been estimated as 3% (Cohen and Gordon, 1978). The uncertainty in the piston velocity has been estimated at 32% (Sweeney et al., 2007). Uncertainties in the solubility and piston velocity are proportional to uncertainty in the optimised N_2O air-sea exchange because the optimised N_2O production needs to change proportionally with solubility and piston velocity to achieve the same ΔpN_2O.

3 Results

3.1 N_2O production at low O_2

The global N_2O production rate in oxygen minimum zones (OMZs) was optimised using the depth-resolved N_2O data of the MEMENTO database. As noted in previous model studies of ocean O_2, global models do not well represent the extent and intensity of OMZ regions (Bopp et al., 2013; Cocco et al., 2013). The modeled OMZs in PlankTOM10 occur at greater depths than observed, resulting in unrealistic vertical distributions of N_2O (results not shown). Therefore, following Suntharalingam et al. (2012), the model was run using fixed observed O_2 concentrations (Bianchi et al., 2012), which corrected, in part, the vertical distribution of N_2O production from the two submodels, though it still occurred at too great depths (Fig. 7). In the equatorial regions and in the Pacific ocean the N_2O concentrations are underestimated between ~200 and ~1500 m. depth, and overestimated below that. This shortcoming is not significantly improved in the prognostic model (Fig. 7), even though the prognostic model is more detailed, separately representing the processes of N_2O production and consumption at low O_2 concentrations. The depth of maximum N_2O in the model is generally deeper than observed, suggesting that organic matter remineralisation may be too low at shallow depths. This is confirmed by the depth profile of NO_3^-, which is underestimated relative to the WOA2009 observations between 100 and 1500 m., and overestimated at greater depths (Fig. 8). In both submodels, the N_2O concentrations in the deep sea are also too high, but since only 5% of N_2O production occurs below 1600 m this does not have a big impact on the global N_2O fluxes. The addition of N_2O consumption in the prognostic N_2O model does result in improvement of the N_2O depth profiles in the Indian Ocean.

In order to find the optimal N_2O production that minimizes the MSE (Eq. 5), we ran a range of simulations in which the low O_2 N_2O production was varied in the diagnostic model (Fig. 9A), and a range of simulations in which both the hypoxic N_2O production and the suboxic N_2O consumption were varied in the prognostic model (Fig. 9B). The optimum solution for the prognostic model was found at a gross production of 0.33 Tg N y^{-1}. The optimised (net) N_2O production in low O_2 regions and its confidence interval were 0.16 ± 0.13 Tg N y^{-1} for the diagnostic model, and 0.12 ± 0.07 Tg N y^{-1} for the prognostic model. In the optimised diagnostic model the hypoxic N_2O ratio (i.e. net production) is 1.7 mmol N_2O (mol O_2)$^{-1}$. In the optimised prognostic model the maximum N_2O production ratio (i.e. gross production from hypoxic denitrification) is 15.4 mmol N_2O (mol NO_3^-)$^{-1}$ decreasing to 0 above 34 μmol O_2 L^{-1}. The maximum N_2O consumption ratio (from suboxic denitrification) is 15 mmol N_2O (mol NO_3^-)$^{-1}$, decreasing to 0 above 28 μmol O_2 L^{-1}. This leads to net production that is always positive and has a maximal ratio of 183 μmol N_2O (mol NO_3^-)$^{-1}$ at 10 μmol O_2 L^{-1}.

3.2 N_2O flux

We used the surface ΔpN_2O distribution to constrain the total global N_2O flux, and the uncertainty arising from the model-data mismatch (the uncertainties arising from solubility and piston velocity are added at the end). We ran a range of simulations in which both the (net) low O_2 and the oxic N_2O production rates were optimised in both submodels (Fig. 10). ΔpN_2O provided a better constraint than the N_2O concentration distribution, since more N_2O production mostly leads to more N_2O outgassing to the atmosphere rather than a significant increase in shallow N_2O concentrations (data not shown). This is because outgassing is proportional to ΔpN_2O, but N_2O concentration is proportional to pN_2O, and $\Delta pN_2O/pN_2O$ is small in most of the surface ocean. The zonal average surface ΔpN_2O distribution was well simulated by both submodels (Fig. 11D), and the model ensemble covered a wide range of global N_2O fluxes (Fig. 10). The total N_2O flux that best reproduced the ΔpN_2O distribution was 2.4 ± 0.3 Tg N y^{-1} for the diagnostic sub-model and 2.5 ± 0.3 Tg N y^{-1} for the prognostic sub-model (Fig. 10). In the diagnostic model, the optimised oxic ΔN_2O/AOU ratio was 10.6 μmol N_2O (mol O_2)$^{-1}$. In the prognostic model, the optimised oxic nitrification ratio was 123 μmol N_2O (mol NH_4^+)$^{-1}$. The results were the same in both diagnostic and prognostic submodels for the 2000-2004 and 2005-2009 averages, showing that the model was sufficiently spun up.

High N_2O fluxes have been reported for the coastal ocean (Bange et al., 1996), and near-shore upwelling regions (e.g. Arevalo-Martinez et al., 2015). To test whether these regions contribute more to the global N_2O flux than their surface area would suggest, we did the optimisation separately for the coastal ocean (≤200 m bottom depth) for the near-shore non-coastal ocean (≤2° from land, >200m bottom depth) for the East Tropical Pacific (180° - 70°W, 5°S - 5°N, >2° from land), and the rest of the open ocean (Table 2). The results show that the coastal ocean contributes only 2% of the global N_2O flux, less than would be expected from its surface area, although there are also fewer observations in the coast (2% of the total) so that the relative error is slightly higher. The near-shore non-coastal ocean contributes 14% of the global N_2O flux both submodels, hardly more than its areal percentage (13%), and it's also fairly well sampled (12% of the observations). The East Equatorial Pacific ocean contributes 27% in the diagnostic submodel and 25% in the prognostic model, more than its areal percentage (22%), and it's undersampled (17%). The open ocean contributes 57 - 59%, slightly less than its areal percentage (61%). This is as expected, because we've separated out the main N_2O hotspots, but the differences are quite small.

When we used observed atmospheric pN_2O that varied with latitude and month (see Sect. 2.2) the results were essentially the same, with an N_2O flux of 2.4 ± 0.3 Tg N y^{-1} for the diagnostic sub-model and 2.6 ± 0.3 Tg N y^{-1} for the prognostic sub-model (data not shown).

Finally, we add the uncertainties in the solubility and the piston velocity to the total N_2O flux through error propagation. This gives a total uncertainty of 2.4 ± 0.8 Tg N y^{-1} for the diagnostic sub-model and 2.5 ± 0.8 Tg N y^{-1} for the prognostic sub-model.

4 Discussion

Cohen and Gordon (1979) estimated global N_2O production directly from N cycle observations as 4 - 10 Tg N y^{-1}. However, they did not have information on the f-ratio, so their estimate was based on total N assimilation in primary production. We use an updated estimate of primary production and its error (Buitenhuis et al., 2013a), and compile a database of the f-ratio (Fig. 2). We also use a much larger database of the ΔN_2O/AOU ratio (Fig. 3). We recalculate the N-cycle-based N_2O production based on these extended databases. We find that we can estimate all the relevant steps in the N cycle with observational data, including their uncertainty (Sect. 2.1). At present this uncertainty is still fairly large, at 4.6 ± 3.1 Tg N y^{-1}. The uncertainty in this estimate is similar to that in Cohen and Gordon (1979), but our uncertainty is based on the uncertainty in all components of the calculation, while their uncertainty was based only on the uncertainty in the ΔN_2O/AOU ratio. The upper 60% of our estimate overlaps with the lower 62% of the Cohen and Gordon (1979) estimate. The biggest contributor to our uncertainty is the f-ratio, especially in the tropics, which constitute 44% of the ocean surface area, and additional measurements and/or data-synthesis could help constrain the N_2O budget. The f-ratio data is only based on uptake of NO_3^-, NH_4^+ and urea, whereas phytoplankton can also take up NO_2^- and organic N (other than urea). One of the major sources of uncertainty in using the $\Delta N_2O/AOU$ ratio is that it is conceptually based on the N_2O production during nitrification, which uses O_2 as the electon acceptor. N_2O production during denitrification is spatially separated from the associated O_2 use that is needed to nitrify the NH_4^+ to NO_3^-, the electron acceptor in denitrification. This NO_3^- is produced by nitrification, so in terms of mass balance our calculation is still valid, but this N_2O production would show up as a vertical increase in N_2O without associated increase in AOU at low O_2 concentrations (high AOU) in Figure 4. This estimate of global marine N_2O production derived from analyzing the N cycle (4.6 ± 3.1 Tg N y^{-1}) is statistically indistinguishable from the N_2O flux derived from ΔpN_2O observations (2.4 - 2.5 ± 0.8 Tg N y^{-1}), but has a much larger error. However, further observational constraints could not only reduce the error, but also extend our understanding of the whole N cycle, including the option of evaluating the model representation of these N cycle processes against observations, and not just the part that N_2O plays in them. Such further constraints are also likely to provide the most productive way to reduce unexplained variability that is found in the observations but not in the present models. E.g., we have shown that both the N_2O and NO_3 are underestimated at ~300 - 1500 m depth and overestimated below ~2000 m (Fig. 6, 7). Thus, improved representation of mesopelagic remineralisation might lead in improved representation of the N_2O depth distribution. However, this falls outside the scope of this study.

Models of the global marine C cycle have been in use for decades, and a lot of the available information has been synthesized, cross-correlated and interpreted in detail (Le Quere et al., 2016a; Buitenhuis et al., 2013b). While actual measurements of N utilisation and transformation have also been made in abundance (Fig. 2, 3, 4, 5A, 6, 7, 9A), the synthesis and global modelling of these data is less advanced. In addition, N occurs in many different oxidation states in the marine environment (e.g. organic matter and NH_4^+ as -3, N_2 as 0, N_2O as 0 and +2, NO_2^- as +3, and NO_3^- as +5). Therefore, redox reactions complicate the representation of the N cycle a good deal. This lack of data synthesis and of identification of the most important controls in a complex system is reflected in a relatively low ability of the model to model observed nitrification rates and to a lesser extent NH_4^+ concentrations (Table 1).

This lack of knowledge also means that partitioning the global marine N_2O production over the nitrification and denitrification pathways is poorly constrained. Both the diagnostic and the prognostic models assign a small percentage of the total N_2O production to the denitrification pathway, 6 and 4% respectively. However, because of the large bias between the observed and modeled N_2O concentration depth profiles (Fig. 7) these may be underestimates (Suntharalingam et al., 2012; Arevalo-Martinez et al., 2015). Possibly because of the model bias (Fig. 7, 8), the addition of N_2O consumption in the prognostic submodel does not lead to a significantly better distribution of N_2O across depth or between different basins (Fig. 8). As a result, the ΔpN_2O distributions are also quite similar (Fig. 11, 12) and the optimised N_2O flux and confidence intervals of the two submodels are also quite similar (Fig. 10). However, it should also be noted, first, that the optimization using surface ΔpN_2O agrees with the optimization using N_2O concentration that the contribution of the low O_2 N_2O production needs to be low (Fig. 10). Second, the error contribution from the model vs. observed ΔpN_2O comparison is low, with confidence intervals of 0.3 Tg N y^{-1} for both submodels. Third, ΔpN_2O is equally well modelled above the low O_2 regions as in the rest of the ocean (Fig. 11, 12), and the contribution of the coastal and near-shore non-coastal ocean are nearly proportional to their surface areas (Table 2). These three features are supporting evidence for our results that suggest that the low O_2 regions make a small contribution to the global ocean N_2O production. They should be balanced against the model bias of the vertical distribution of N_2O concentrations, which suggests a larger contribution from the low O_2 regions. Freing et al. (2012) also estimated a small fraction of 7% of the global total contributed by denitrification / low O_2 N_2O production. Two complementary approaches could provide better constraints: a better representation of the vertical distribution of export and remineralisation would allow the optimization against N_2O concentration observations to achieve better results. But conversely, with better constraints on the physiology of nitrifiers and denitrifiers the N_2O concentration database could provide constraints on the representation of remineralisation. Although there are relatively few N_2O concentration observations, nitrification and denitrification respond to specific environmental queues (in particular O_2 concentration), so that the they could contribute a relatively large observational constraint over the full range of environmental conditions.

Despite these shortcomings, the global marine N_2O flux is well constrained to 2.4 - 2.5 ± 0.8 Tg N y^{-1} by both submodels (Fig. 10). This constraint reflects the fact that the integrated effect of the different physical and biogeochemical processes determines the surface ΔpN_2O distribution (Fig. 11), so that the integrated total can be well constrained even if the individual processes are not. The N_2O flux is at the lower end of previous estimates, and with a similar confidence interval to other recent estimates (Fig. 4). The confidence interval is dominated by uncertainty in the piston velocity (32%) rather than model-observation mismatches (12%). Because of differences in methodology it is not possible to provide reasons for why our estimate is lower than the more recent estimates. We can, however, compare our estimate to that of (Nevison et al., 1995), because it is also based on a database of ΔpN_2O. Compared to their high end estimate using the piston velocity of Wanninkhof of 5.2 ± 3.6 Tg N y^{-1}, our estimate is lower because we use the more recent 13% lower estimate of piston velocity of (Sweeney et al., 2007), and because our ΔpN_2O of 7.6 ± 18.1 ppb is 25 - 28% lower compared to 10.55 natm in Nevison et al. (1995) (the range is calculated based on the water vapor correction for conversion between ppb and natm, which increases from 0.6 - 4.1% at temperatures from 0 - 30 °C, which brings the values slightly closer together).

We also tested how much influence sampling biases of very high supersaturation values might have on the estimated air-sea exchange. If the 40 ΔpN_2O measurements in the gridded database that are higher than 100 ppb (Fig. 12) are doubled, the optimised N_2O air-sea exchange becomes 2.8 ± 0.5 Tg N y^{-1} for the diagnostic model and 3.1 ± 0.5 Tg N y^{-1} for the prognostic model. If the 24 ΔpN_2O measurements in the gridded database that are higher than 152 ppm are excluded, to decrease the frequency of the highly oversaturated observations down to what both submodels simulate (Fig. 12), the optimised N_2O flux become 2.0 ± 0.2 for the diagnostic model and 2.3 ± 0.2 Tg N y^{-1} for the prognostic model. These results still fall within the confidence intervals of the results using the complete database.

Possible biases in ocean physical transport could in theory affect N_2O production in low O_2 regions. The indirect impact of ocean physics on low N_2O production through its impact on the distribution of O_2, which Zamora and Oschlies (2014) have shown to be substantial, is not quantified here because we used observed O_2 (Bianchi et al., 2012) instead of modeled O_2. Our model results suggest that the model representation of ocean physics is adequate for the purpose of estimating N_2O flux from biogeochemical model perturbations. On the one hand, if the model had too much ventilation in the OMZs, shallow N_2O concentrations would be underestimated, as they are in the model (Fig. 7), but this would also lead to ΔpN_2O overestimation in the surface areas above the OMZs, which is not the case. The high ΔpN_2O are generally lower but spread over a larger area than in the observations (Fig. 11), with a good frequency distribution of high ΔpN_2O (Fig. 12). On the other hand, if the model had too little ventilation in the OMZs, the optimization would reduce N_2O production in the OMZs in compensation, but the optimization to ΔpN_2O would then estimate a higher OMZ N_2O production than the optimization to the N_2O depth profiles to compensate for the low transport, and this is also not the case. Therefore we conclude that potential biases in ocean physical transport do not appear to have a large direct impact on low N_2O production.

Global oceanic N_2O emissions estimated using atmospheric inversion methods based on atmospheric N_2O concentrations tend to be higher than our results (Fig. 4). However, N_2O emissions from inversions in the Southern Ocean are lower than the priors (Hirsch et al., 2006; Huang et al., 2008; Thompson et al., 2014; Saikawa et al., 2014). These low Southern Ocean emissions (0.02 - 0.72 Tg N y^{-1}) are consistent with our results (0.68 - 0.79 Tg N y^{-1}). South of 30°S, 88% of the Earth surface is ocean, resulting in a clearer attribution in the inversions of the atmospheric N_2O anomalies to ocean fluxes. We suggest that the higher emissions estimates from inversions for the global ocean could be due to a combination of overestimated priors of ocean fluxes in combination with insufficient observational constraints at latitudes North of 30°S to allow correct partitioning between land and ocean fluxes. Results presented here are for the open and coastal ocean. The largest coastal seas are resolved in our model, although specific coastal processes, such as the interactions with sediments and tides, are not. Our results do not include emissions from estuaries. Fluxes from these could be as large as 2.3 - 3.6 Tg N y^{-1} according to one estimate (Bange et al., 1996), and could be another contributing factor to the difference between our results and those of atmospheric inversions.

To improve the estimate of the ocean N_2O flux, first, the uncertainty in the piston velocity would need to be reduced. Once that is achieved, further improvements might be possible by a more accurate model representations of the remineralisation length scale and of the physiology of N_2O producing picoheterotrophs (nitrifying and denitrifying *Archaea* and *Bacteria*).

Code and data availability. The four databases presented in this manuscript are available as NetCDF files from https://www.uea.ac.uk/green-ocean/data. The code of PlankTOM10.2 is available at greenocean-data.uea.ac.uk/model/PlankTOM10.2.tar

Competing interests. The authors declare they have no competing interests.

Acknowledgements. This research was supported by the European Commission's Horizon 2020 programme through the CRESCENDO and EMBRACE projects (projects 641816 and 282672). We thank Martin Johnson for the database of NH_4^+, and Andrew Yool for the database of nitrification rates. The MEMENTO database is administered by the Kiel Data Management Team at GEOMAR Helmholtz Centre for Ocean Research and supported by the German BMBF project SOPRAN (Surface Ocean Processes in the Anthropocene, http://sopran.pangaea.de).

We thank Alina Freing for providing the corrected numbers for the polynomial fit to the atmospheric pN2O data, and NOAA for providing atmospheric pN2O data.

References

Aksnes, D. and Egge, J.: A theoretical-model for nutrient-uptake in phytoplankton, Marine ecology progress series, 70, 65–72, doi:10.3354/meps070065, 1991.

Anderson, L. and Sarmiento, J.: Redfield ratios of remineralization determined by nitrient data-analysis, Global biogeochemical cycles, 8, 65–80, doi:10.1029/93GB03318, 1994.

Arevalo-Martinez, D. L., Kock, A., Loescher, C. R., Schmitz, R. A., and Bange, H. W.: Massive nitrous oxide emissions from the tropical South Pacific Ocean, Nature Geoscience, 8, 530–U168, doi:10.1038/NGEO2469, 2015.

Babbin, A. R., Bianchi, D., Jayakumar, A., and Ward, B. B.: Rapid nitrous oxide cycling in the suboxic ocean, Science, 348, 1127–1129, doi:10.1126/science.aaa8380, 2015.

Bange, H.: Gaseous nitrogen compounds (NO, N2O, N2, NH3) in the ocean, in: Nitrogen in the marine environment, edited by Capone, DG and Bronk, DA and Mulholland, MR and Carpenter, EJ, pp. 51–94, 2008.

Bange, H., Rapsomanikis, S., and Andreae, M.: Nitrous oxide in coastal waters, Global biogeochemical cycles, 10, 197–207, doi:10.1029/95GB03834, 1996.

Bange, H. W., Bell, T. G., Cornejo, M., Freing, A., Uher, G., Upstill-Goddard, R. C., and Zhang, G.: MEMENTO: a proposal to develop a database of marine nitrous oxide and methane measurements, Environmental chemistry, 6, 195–197, doi:10.1071/EN09033, 2009.

Bianchi, D., Dunne, J. P., Sarmiento, J. L., and Galbraith, E. D.: Data-based estimates of suboxia, denitrification, and N2O production in the ocean and their sensitivities to dissolved O-2, Global biogeochemical cycles, 26, doi:10.1029/2011GB004209, 2012.

Bopp, L., Resplandy, L., Orr, J. C., Doney, S. C., Dunne, J. P., Gehlen, M., Halloran, P., Heinze, C., Ilyina, T., Seferian, R., Tjiputra, J., and Vichi, M.: Multiple stressors of ocean ecosystems in the 21st century: projections with CMIP5 models, Biogeosciences, 10, 6225–6245, doi:10.5194/bg-10-6225-2013, 2013.

Buitenhuis, E., Le Quere, C., Aumont, O., Beaugrand, G., Bunker, A., Hirst, A., Ikeda, T., O'Brien, T., Piontkovski, S., and Straile, D.: Biogeochemical fluxes through mesozooplankton, Global biogeochemical cycles, 20, doi:10.1029/2005GB002511, 2006.

Buitenhuis, E. T., Rivkin, R. B., Sailley, S., and Le Quere, C.: Biogeochemical fluxes through microzooplankton, Global biogeochemical cycles, 24, doi:10.1029/2009GB003601, 2010.

Buitenhuis, E. T., Hashioka, T., and Le Quere, C.: Combined constraints on global ocean primary production using observations and models, Global biogeochemical cycles, 27, 847–858, doi:10.1002/gbc.20074, 2013a.

Buitenhuis, E. T., Vogt, M., Moriarty, R., Bednarsek, N., Doney, S. C., Leblanc, K., Le Quere, C., Luo, Y. W., O'Brien, C., O'Brien, T., Peloquin, J., Schiebel, R., and Swan, C.: MAREDAT: towards a world atlas of MARine Ecosystem DATa, Earth system science data, 5, 227–239, doi:10.5194/essd-5-227-2013, 2013b.

Butler, J., Elkins, J., Thompson, T., and Egan, K.: Trophospheric and dissolved N2O of the West Pacific and East-Indian Oceans during the El-Nino Southern Oscillation event of 1987, Journal of geophysical research-Atmospheres, 94, 14 865–14 877, doi:10.1029/JD094iD12p14865, 1989.

Ciais, P., Sabine, C., Bala, G., Bopp, L., Brovkin, V., Canadell, J., Chhabra, A., DeFries, R., Heimann, M., Jones, C., Le Quere, C., Myneni, B., Piao, S., and Thornton, P.: Carbon and other biogeochemical cycles, in: Climate change 2013: The physical science basis, edited by Stocker, TF and Qin, D and Plattner, M and Tignor, M and Allen, SK and Boschung, J and Nauels, Y and Xia, Y and Bex, V and Midgley, PM, pp. 465–570, doi:10.1017/CBO9781107415324.015, 2013.

Cocco, V., Joos, F., Steinacher, M., Froelicher, T. L., Bopp, L., Dunne, J., Gehlen, M., Heinze, C., Orr, J., Oschlies, A., Schneider, B., Segschneider, J., and Tjiputra, J.: Oxygen and indicators of stress for marine life in multi-model global warming projections, Biogeosciences, 10, 1849–1868, doi:10.5194/bg-10-1849-2013, 2013.

Cohen, Y. and Gordon, L.: Nitrous-oxide in oxygen minimum of eastern tropical North Pacific - evidence for its consumption during denitrification and possible mechanisms for its production, Deep-sea research, 25, 509–524, doi:10.1016/0146-6291(78)90640-9, 1978.

Cohen, Y. and Gordon, L.: Nitrous-oxide production in the ocean, Journal of geophysical research-Oceans and atmospheres, 84, 347–353, doi:10.1029/JC084iC01p00347, 1979.

Frame, C. H. and Casciotti, K. L.: Biogeochemical controls and isotopic signatures of nitrous oxide production by a marine ammonia-oxidizing bacterium, Biogeosciences, 7, 2695–2709, doi:10.5194/bg-7-2695-2010, 2010.

Francis, C., Roberts, K., Beman, J., Santoro, A., and Oakley, B.: Ubiquity and diversity of ammonia-oxidizing archaea in water columns and sediments of the ocean, Proceedings of the national academy of sciences of the United States of America, 102, 14 683–14 688, doi:10.1073/pnas.0506625102, 2005.

Freing, A., Wallace, D. W. R., Tanhua, T., Walter, S., and Bange, H. W.: North Atlantic production of nitrous oxide in the context of changing atmospheric levels, Global biogeochemical cycles, 23, doi:10.1029/2009GB003472, 2009.

Freing, A., Wallace, D. W. R., and Bange, H. W.: Global oceanic production of nitrous oxide, Philosophical transactions of the royal society B-biological sciences, 367, 1245–1255, doi:10.1098/rstb.2011.0360, 2012.

Gandhi, N., Prakash, S., Ramesh, R., and Kumar, S.: Nitrogen uptake rates and new production in the northern Indian Ocean, Indian journal of marine sciences, 39, 362–368, 2010.

Gandhi, N., Ramesh, R., Laskar, A. H., Sheshshayee, M. S., Shetye, S., Anilkumar, N., Patil, S. M., and Mohan, R.: Zonal variability in primary production and nitrogen uptake rates in the southwestern Indian Ocean and the Southern Ocean, Deep-sea research part I-Oceanographic research papers, 67, 32–43, doi:10.1016/j.dsr.2012.05.003, 2012.

Goldman, J. and PM, G.: Kinetics of inorganic nitrogen uptake by phytoplankton, in: Nitrogen in the marine environment, edited by Carpenter, EJ and Capone, DG, 1983.

Goreau, T., Kaplan, W., Wofsy, S., McElroy, M., Valois, F., and Watson, S.: Production of NO2- and N2O by nitrifying bacteria at reduced concentrations of oxygen, Applied and environmental microbiology, 40, 526–532, 1980.

Hirsch, A., Michalak, A., Bruhwiler, L., Peters, W., Dlugokencky, E., and Tans, P.: Inverse modeling estimates of the global nitrous oxide surface flux from 1998-2001, Global biogeochemical cycles, 20, doi:10.1029/2004GB002443, 2006.

Horrigan, S., Carlucci, A., and Williams, P.: Light inhibition of nitrification in sea-surface films, Journal of marine research, 39, 557–565, 1981.

Huang, J., Golombek, A., Prinn, R., Weiss, R., Fraser, P., Simmonds, P., Dlugokencky, E. J., Hall, B., Elkins, J., Steele, P., Langenfelds, R., Krummel, P., Dutton, G., and Porter, L.: Estimation of regional emissions of nitrous oxide from 1997 to 2005 using multinetwork measurements, a chemical transport model, and an inverse method, Journal of geophysical research-Atmospheres, 113, doi:10.1029/2007JD009381, 2008.

Jin, X. and Gruber, N.: Offsetting the radiative benefit of ocean iron fertilization by enhancing N2O emissions, Geophysical research letters, 30, doi:10.1029/2003GL018458, 2003.

Joubert, W. R., Thomalla, S. J., Waldron, H. N., Lucas, M. I., Boye, M., Le Moigne, F. A. C., Planchon, F., and Speich, S.: Nitrogen uptake by phytoplankton in the Atlantic sector of the Southern Ocean during late austral summer, Biogeosciences, 8, 2947–2959, doi:10.5194/bg-8-2947-2011, 2011.

Kalnay, E., Kanamitsu, M., Kistler, R., Collins, W., Deaven, D., Gandin, L., Iredell, M., Saha, S., White, G., Woollen, J., Zhu, Y., Chelliah, M., Ebisuzaki, W., Higgins, W., Janowiak, J., Mo, K., Ropelewski, C., Wang, J., Leetmaa, A., Reynolds, R., Jenne, R., and Joseph, D.: The NCEP/NCAR 40-year reanalysis project, Bulletine of the American meteorological society, 77, 437–471, doi:10.1175/1520-0477(1996)077<0437:TNYRP>2.0.CO;2, 1996.

Killberg-Thoreson, L., Mulholland, M. R., Heil, C. A., Sanderson, M. P., O'Neil, J. M., and Bronk, D. A.: Nitrogen uptake kinetics in field populations and cultured strains of Karenia brevis, Harmful Algae, 38, 73–85, doi:10.1016/j.hal.2014.04.008, 2014.

Klawonn, I., Bonaglia, S., Bruchert, V., and Ploug, H.: Aerobic and anaerobic nitrogen transformation processes in N-2-fixing cyanobacterial aggregates, ISME Journal, 9, 1456–1466, doi:10.1038/ismej.2014.232, 2015.

Kock, A. and Bange, H.: Counting the ocean's greenhouse gas emissions, EOS, 96, 10–13, doi:10.1029/2015EO023665, 2015.

Law, C. and Owens, N.: Significant flux of atmospheric nitrous-oxide from the Northwest Indian-Ocean, Nature, 346, 826–828, doi:10.1038/346826a0, 1990.

Le Quere, C., Andrew, R. M., Canadell, J. G., Sitch, S., Korsbakken, J. I., Peters, G. P., Manning, A. C., Boden, T. A., Tans, P. P., Houghton, R. A., Keeling, R. F., Alin, S., Andrews, O. D., Anthoni, P., Barbero, L., Bopp, L., Chevallier, F., Chini, L. P., Ciais, P., Currie, K., Delire, C., Doney, S. C., Friedlingstein, P., Gkritzalis, T., Harris, I., Hauck, J., Haverd, V., Hoppema, M., Goldewijk, K. K., Jain, A. K., Kato, E., Koertzinger, A., Landschuetzer, P., Lefevre, N., Lenton, A., Lienert, S., Lombardozzi, D., Melton, J. R., Metzl, N., Millero, F., Monteiro, P. M. S., Munro, D. R., Nabel, J. E. M. S., Nakaoka, S.-i., O'Brien, K., Olsen, A., Omar, A. M., Ono, T., Pierrot, D., Poulter, B., Roedenbeck, C., Salisbury, J., Schuster, U., Schwinger, J., Seferian, R., Skjelvan, I., Stocker, B. D., Sutton, A. J., Takahashi, T., Tian, H., Tilbrook, B., van der Laan-Luijkx, I. T., van der Werf, G. R., Viovy, N., Walker, A. P., Wiltshire, A. J., and Zaehle, S.: Global Carbon Budget 2016, Earth system science data, 8, 605–649, doi:10.5194/essd-8-605-2016, 2016a.

Le Quere, C., Buitenhuis, E. T., Moriarty, R., Alvain, S., Aumont, O., Bopp, L., Chollet, S., Enright, C., Franklin, D. J., Geider, R. J., Harrison, S. P., Hirst, A. G., Larsen, S., Legendre, L., Platt, T., Prentice, I. C., Rivkin, R. B., Sailley, S., Sathyendranath, S., Stephens, N., Vogt, M., and Vallina, S. M.: Role of zooplankton dynamics for Southern Ocean phytoplankton biomass and global biogeochemical cycles, Biogeosciences, 13, 4111–4133, doi:10.5194/bg-13-4111-2016, 2016b.

Lipschultz, F., Zafiriou, O., Wofsy, S., McElroy, M., Valois, F., and Watson, S.: Production of NO and N2O by soil nitrifying bacteria, Nature, 294, 641–643, doi:10.1038/294641a0, 1981.

Loescher, C. R., Kock, A., Koenneke, M., LaRoche, J., Bange, H. W., and Schmitz, R. A.: Production of oceanic nitrous oxide by ammonia-oxidizing archaea, Biogeosciences, 9, 2419–2429, doi:10.5194/bg-9-2419-2012, 2012.

Madec, G.: NEMO ocean engine., vol. No. 27, Institute Pierre-Simon Laplace (IPSL), 2008.

Martinez-Rey, J., Bopp, L., Gehlen, M., Tagliabue, A., and Gruber, N.: Projections of oceanic N2O emissions in the 21st century using the IPSL Earth system model, Biogeosciences, 12, 4133–4148, doi:10.5194/bg-12-4133-2015, 2015.

Merbt, S. N., Stahl, D. A., Casamayor, E. O., Marti, E., Nicol, G. W., and Prosser, J. I.: Differential photoinhibition of bacterial and archaeal ammonia oxidation, FEMS microbiology letters, 327, 41–46, doi:10.1111/j.1574-6968.2011.02457.x, 2012.

Morel, F.: Kinetics of nutrient-uptake and growth in phytoplankton, Journal of Phycology, 23, 137–150, 1987.

Myhre, G., Shindell, D., Breon, F., Collins, W., Fuglestyedt, J., Huang, J., Koch, D., Lamarque, J., Lee, D., Mendoza, T., Nakajima, A., Robock, A., Stephens, G., Takemura, T., and Zhang, H.: Anthropogenic and natural radiative forcing, in: Climate change 2013: The physical science basis, edited by Stocker, TF and Qin, D and Plattner, M and Tignor, M and Allen, SK and Boschung, J and Nauels, Y and Xia, Y and Bex, V and Midgley, PM, pp. 659–740, doi:10.1017/CBO9781107415324.018, 2013.

Nevison, C., Weiss, R., and Erickson, D.: Global oceanic emissions of nitrous-oxide, Journal of geophysical research-Oceans, 100, 15 809–15 820, doi:10.1029/95JC00684, 1995.

Nevison, C., Butler, J., and Elkins, J.: Global distribution of N2O and the Delta N2O-AOU yield in the subsurface ocean, Global biogeochemical cycles, 17, doi:10.1029/2003GB002068, 2003.

Paulot, F., Jacob, D. J., Johnson, M. T., Bell, T. G., Baker, A. R., Keene, W. C., Lima, I. D., Doney, S. C., and Stock, C. A.: Global oceanic emission of ammonia: Constraints from seawater and atmospheric observations, Global biogeochemical cycles, 29, 1165–1178, doi:10.1002/2015GB005106, 2015.

Portmann, R. W., Daniel, J. S., and Ravishankara, A. R.: Stratospheric ozone depletion due to nitrous oxide: influences of other gases, Philosophical transactions of the royal society B-biological sciences, 367, 1256–1264, doi:10.1098/rstb.2011.0377, 2012.

Prakash, S., Ramesh, R., Sheshshayee, M. S., Dwivedi, R. M., and Raman, M.: Quantification of new production during a winter Noctiluca scintillans bloom in the Arabian Sea, Geophysical research letters, 35, doi:10.1029/2008GL033819, 2008.

Prakash, S., Ramesh, R., Sheshshayee, M. S., Mohan, R., and Sudhakar, M.: Nitrogen uptake rates and f-ratios in the Equatorial and Southern Indian Ocean, Current science, 108, 239–245, 2015.

Qin, W., Amin, S. A., Martens-Habbena, W., Walker, C. B., Urakawa, H., Devol, A. H., Ingalls, A. E., Moffett, J. W., Armbrust, E. V., and Stahl, D. A.: Marine ammonia-oxidizing archaeal isolates display obligate mixotrophy and wide ecotypic variation, Proceedings of the national academy of sciences of the United States of America, 111, 12 504–12 509, doi:10.1073/pnas.1324115111, 2014.

Saikawa, E., Prinn, R. G., Dlugokencky, E., Ishijima, K., Dutton, G. S., Hall, B. D., Langenfelds, R., Tohjima, Y., Machida, T., Manizza, M., Rigby, M., O'Doherty, S., Patra, P. K., Harth, C. M., Weiss, R. F., Krummel, P. B., van der Schoot, M., Fraser, P. J., Steele, L. P., Aoki, S., Nakazawa, T., and Elkins, J. W.: Global and regional emissions estimates for N2O, Atmospheric chemistry and physics, 14, 4617–4641, doi:10.5194/acp-14-4617-2014, 2014.

Sarmiento, J., Orr, J., and Siegenthaler, U.: A perturbation simulation of CO2 uptake in an ocean general-cirulation model, Journal of geophysical research-Oceans, 97, 3621–3645, doi:10.1029/91JC02849, 1992.

Simpson, K. G., Tremblay, J.-E., Brugel, S., and Price, N. M.: Nutrient dynamics in the western Canadian Arctic. II. Estimates of new and regenerated production over the Mackenzie Shelf and Cape Bathurst Polynya, Marine ecology progress series, 484, 47–62, doi:10.3354/meps10298, 2013.

Stawiarski, B.: The physiological response of picophytoplankton to light, temperature and nutrients, including climate change model simulations, Ph.D. thesis, University of East Anglia, 2014.

Suntharalingam, P. and Sarmiento, J.: Factors governing the oceanic nitrous oxide distribution: Simulations with an ocean general circulation model, Global biogeochemical cycles, 14, 429–454, doi:10.1029/1999GB900032, 2000.

Suntharalingam, P., Sarmiento, J., and Toggweiler, J.: Global significance of nitrous-oxide production and transport from oceanic low-oxygen zones: A modeling study, Global biogeochemical cycles, 14, 1353–1370, doi:10.1029/1999GB900100, 2000.

Suntharalingam, P., Buitenhuis, E., Le Quere, C., Dentener, F., Nevison, C., Butler, J. H., Bange, H. W., and Forster, G.: Quantifying the impact of anthropogenic nitrogen deposition on oceanic nitrous oxide, Geophysical research letters, 39, doi:10.1029/2011GL050778, 2012.

Sweeney, C., Gloor, E., Jacobson, A. R., Key, R. M., McKinley, G., Sarmiento, J. L., and Wanninkhof, R.: Constraining global air-sea gas exchange for CO2 with recent bomb C-14 measurements, Global biogeochemical cycles, 21, doi:10.1029/2006GB002784, 2007.

Thomalla, S. J., Waldron, H. N., Lucas, M. I., Read, J. F., Ansorge, I. J., and Pakhomov, E.: Phytoplankton distribution and nitrogen dynamics in the southwest indian subtropical gyre and Southern Ocean waters, Ocean science, 7, 113–127, doi:10.5194/os-7-113-2011, 2011.

Thompson, R. L., Chevallier, F., Crotwell, A. M., Dutton, G., Langenfelds, R. L., Prinn, R. G., Weiss, R. F., Tohjima, Y., Nakazawa, T., Krummel, P. B., Steele, L. P., Fraser, P., O'Doherty, S., Ishijima, K., and Aoki, S.: Nitrous oxide emissions 1999 to 2009 from a global atmospheric inversion, Atmospheric chemistry and physics, 14, 1801–1817, doi:10.5194/acp-14-1801-2014, 2014.

Vallina, S. M. and Le Quere, C.: Preferential uptake of NH4+ over NO32- in marine ecosystem models: A simple and more consistent parameterization, Ecological modelling, 218, 393–397, doi:10.1016/j.ecolmodel.2008.06.038, 2008.

Varela, D. E., Crawford, D. W., Wrohan, I. A., Wyatt, S. N., and Carmack, E. C.: Pelagic primary productivity and upper ocean nutrient dynamics across Subarctic and Arctic Seas, Journal of geophysical research-Oceans, 118, 7132–7152, doi:10.1002/2013JC009211, 2013.

Varela, M., Bode, A., Fernandez, E., Gonzalez, N., Kitidis, V., Varela, M., and Woodward, E.: Nitrogen uptake and dissolved organic nitrogen release in planktonic communities characterised by phytoplankton size-structure in the Central Atlantic Ocean, Deep-sea research part I-Oceanographic research papers, 52, 1637–1661, doi:10.1016/j.dsr.2005.03.005, 2005.

Wafar, M., L'Helguen, S., Raikar, V., Maguer, J., and Corre, P.: Nitrogen uptake by size-fractionated plankton in permanently well-mixed temperate coastal waters, Journal of plankton research, 26, 1207–1218, doi:10.1093/plankt/fbh110, 2004.

Wanninkhof, R.: Relationship between wind-speed and gas-exchange over the ocean, Journal of geophysical research-Oceans, 97, 7373–7382, doi:10.1029/92JC00188, 1992.

Weiss, R. and Price, B.: Nitrous-oxide solubility in water and seawater, Marine chemistry, 8, 347–359, doi:10.1016/0304-4203(80)90024-9, 1980.

Wuchter, C., Abbas, B., Coolen, M. J. L., Herfort, L., van Bleijswijk, J., Timmers, P., Strous, M., Teira, E., Herndl, G. J., Middelburg, J. J., Schouten, S., and Damste, J. S. S.: Archaeal nitrification in the ocean, Proceedings of the national academy of sciences of the United States of America, 103, 12 317–12 322, doi:10.1073/pnas.0600756103, 2006.

Yool, A., Martin, A. P., Fernandez, C., and Clark, D. R.: The significance of nitrification for oceanic new production, Nature, 447, 999–1002, doi:10.1038/nature05885, 2007.

Yoshida, N., Morimoto, H., Hirano, M., Koike, I., Matsua, S., Wada, E., Saino, T., and Hattori, A.: Nitrification rates and N-15 abundances of N2O and NO3 in the western North Pacific, Nature, 342, 895–897, doi:10.1038/342895a0, 1989.

Yoshinari, T.: Nitrous oxide in the sea, Marine Chemistry, 4, 189–202, 1976.

Zamora, L. M. and Oschlies, A.: Surface nitrification: A major uncertainty in marine N2O emissions, Geophysical research letters, 41, 4247–4253, doi:10.1002/2014GL060556, 2014.

Table 1. Cost function (Eq. 3) for the optimisation simulations of sections 2.2-2.4, relative to the respective observational databases. The nitrification rate in bold was used in this study.

Database	Model change	Cost function
Nitrification rate	0.2 d^{-1}	4.22
	0.1 d^{-1} × 2$^{(T/10)}$	4.18
	0.79 d^{-1} × 2$^{(T/10)}$ × (1 - 0.159 × ln(O$_2$))	**4.16**
	0.58 d^{-1} × 2$^{(T/10)}$ × e$^{(-0.14 \times I)}$	7.15
	4.7 d^{-1} × 2$^{(T/10)}$ × (1 - 0.159 × ln(O$_2$)) × e$^{(-0.14 \times I)}$	6.87
Surface NH_4^+ concentration	$K_{1/2}$ estimated from observations	3.0

Table 2. Contributions of coastal (bottom depth $\leq$ 200 m), near-shore non-coastal ($\leq$ 2° from land, bottom depth > 200 m), East equatorial Pacific (180° - 70°W 5°S - 5°N, >2° from land) and rest of the open ocean (>2° from land, bottom depth > 200 m, excluding East Eq. Pac.) to N_2O flux, area and number of observations.

Region	Submodel	N_2O flux	% N_2O flux	% area	% n_{obs}
Coastal ocean	Diagnostic	0.05 ± 0.01	2	5	2
	Prognostic	0.041 ± 0.007	2		
Deep offshore	Diagnostic	0.33 ± 0.04	14	13	12
	Prognostic	0.37 ± 0.04	14		
East Eq. Pac.	Diagnostic	0.64 ± 0.05	27	22	17
	Prognostic	0.67 ± 0.05	25		
Open ocean	Diagnostic	1.37 ± 0.19	57	61	69
	Prognostic	1.54 ± 0.21	59		

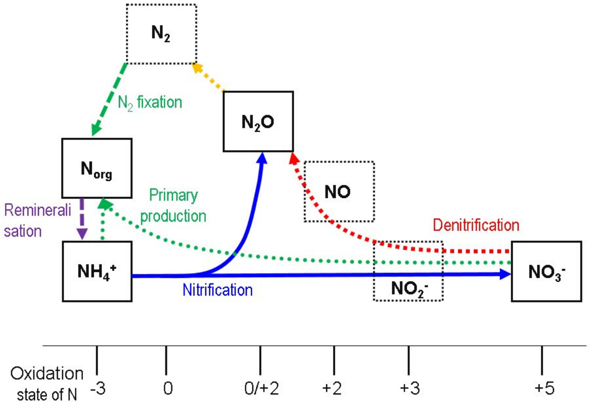

Figure 1. Primary biological pathways of the oceanic nitrogen cycle represented in the model simulations, along with redox states of N. Nitrification occurs in the oxic ocean (blue arrow). Denitrification yields net N_2O production in hypoxic conditions (red arrow) and net N_2O consumption in suboxic conditions (yellow arrow). Only organic nitrogen (N_{org}), NH_4^+, NO_3^- and N_2O are represented as model state variables.

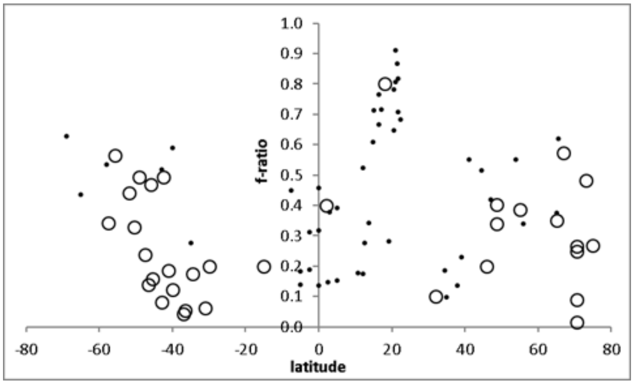

Figure 2. f-ratio ($\rho_{NO_3^-}$/($\rho_{NO_3^-}$+$\rho_{NH_4^+}$+ρ_{urea})) as a function of latitude, from ^{15}N uptake experiments. Small dots were estimated without measuring NH_4^+ or urea concentrations (Prakash et al., 2008, 2015; Gandhi et al., 2010, 2012). Large dots did not give a significant linear relationship with absolute value of latitude, and were therefore averaged at 0.29 ± 0.18 (Wafar et al., 2004; Varela et al., 2005, 2013; Joubert et al., 2011; Thomalla et al., 2011; Simpson et al., 2013).

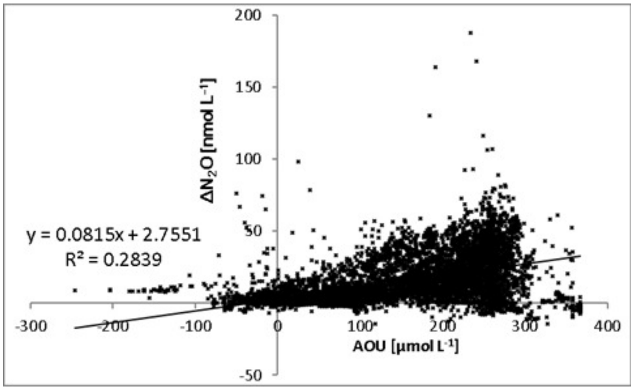

Figure 3. Apparent N_2O production (ΔN_2O nmol L^{-1}) as a function of apparent oxygen utilization (AOU μmol L^{-1}).

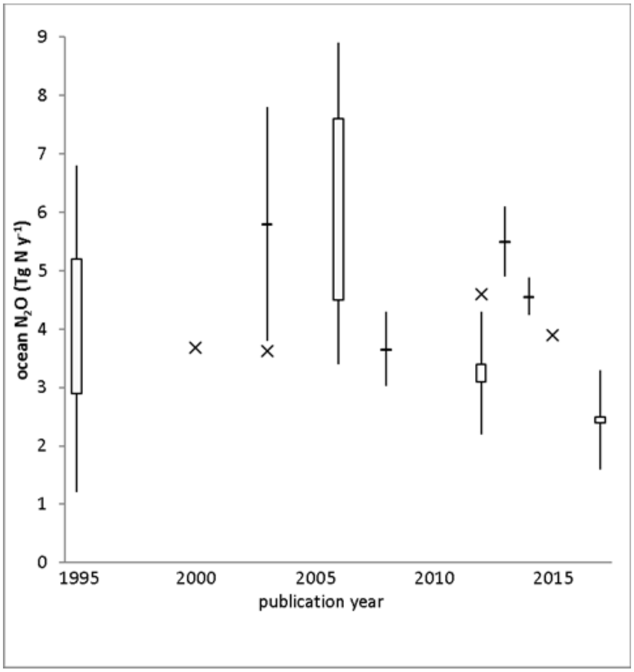

Figure 4. Published estimates of global ocean N_2O production or air-sea exchange. Estimates based on global observational datasets shown as boxes when ranges are given and whiskers if error estimates are given (ocean observations: Nevison et al. (1995, 2003); Freing et al. (2012) (plotted in 2011), Bianchi et al. (2012), this study; atmospheric inversions: Hirsch et al. (2006); Huang et al. (2008); Thompson et al. (2014) (plotted in 2013), Saikawa et al. (2014)), model estimates shown as crosses (Suntharalingam and Sarmiento (2000); Jin and Gruber (2003); Suntharalingam et al. (2012); Martinez-Rey et al. (2015)).

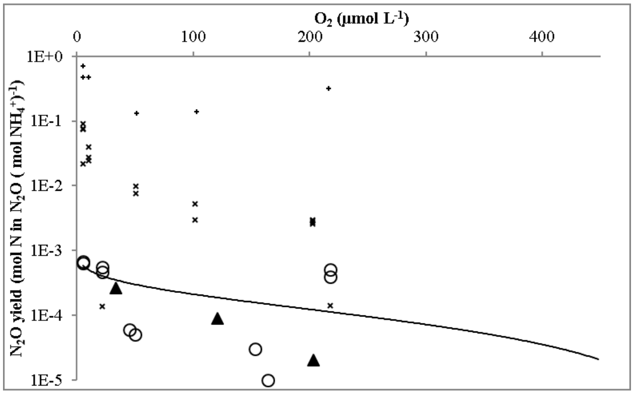

Figure 5. N_2O yield of nitrification (N atom:atom) as a function of O_2 concentration, filled triangles: AOA (Loescher et al., 2012), open circles: AOB at low to medium cell numbers (Frame and Casciotti, 2010; Loescher et al., 2012), crosses: marine AOB at high cell numbers (Goreau et al., 1980; Frame and Casciotti, 2010), plusses: soil AOB at high cell numbers (Lipschultz et al., 1981). Black line: logarithmic fit to AOA and low to medium cell number AOB (yield = 0.791-0.126·ln(O_2) mmol N in N_2O (mol NH_4^+)$^{-1}$).

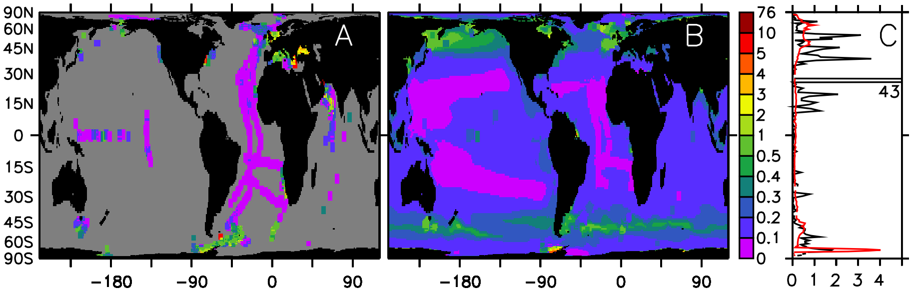

Figure 6. Surface NH_4^+ concentration (μmol L^{-1}). A) observations (symbol size is 5 × 5°). B) model results are for the same months where there are observations, and annual averages everywhere else. C) zonal average, black) observations, red) model results. Model results are for the same months and longitudes as the observations. Latitude y-axis to the left of panel A.

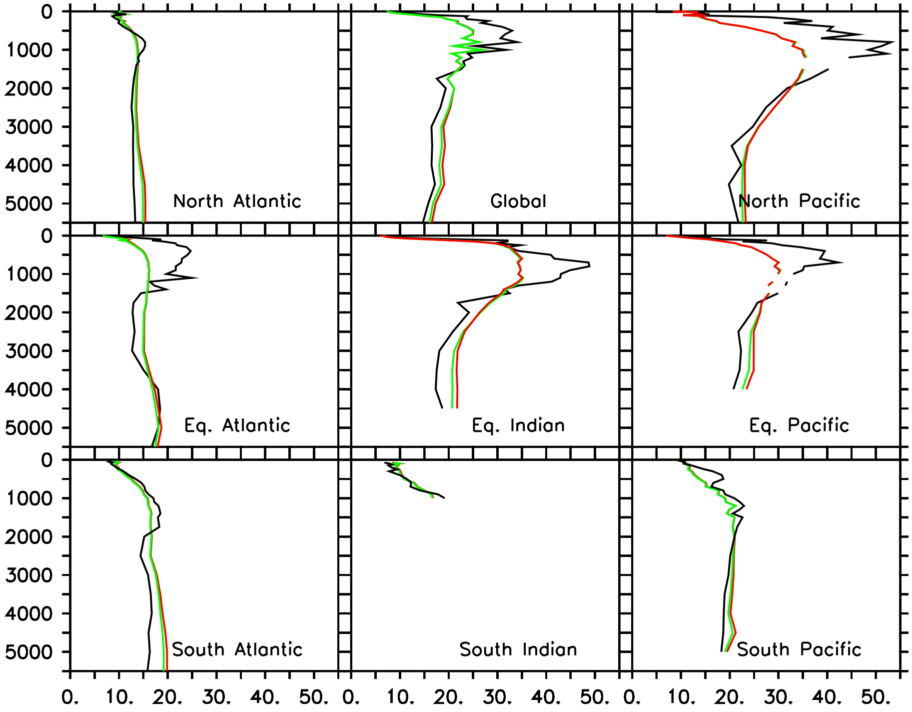

Figure 7. Depth profiles of N_2O concentration (nmol L^{-1}) for different basins. Black lines: observations, Green lines: optimised diagnostic model, Red lines: optimised prognostic model.

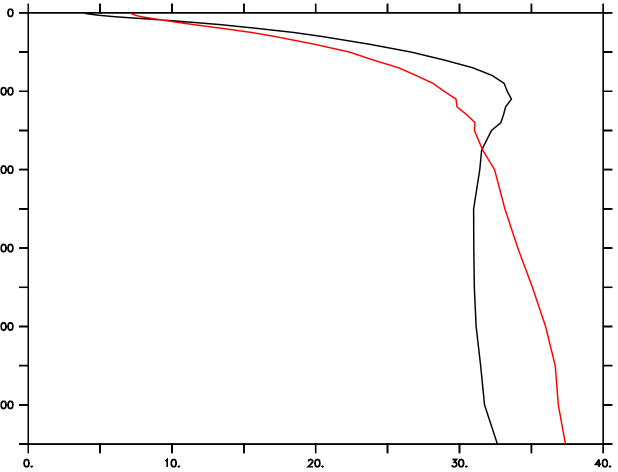

Figure 8. Depth (m.) profile of average NO_3^- concentration (μmol L^{-1}). Black line) WOA2009 synthesis of observations, not interpolated. Red line) Model results sampled at the places where there are observations.

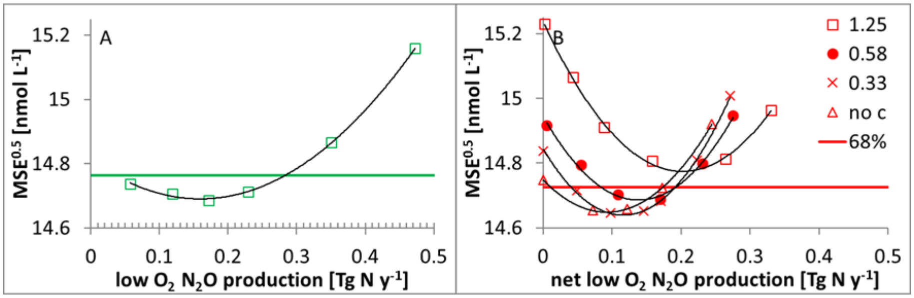

Figure 9. MSE$^{0.5}$ for the two N$_2$O submodels compared to the N$_2$O concentration database as a function N$_2$O production in the low O$_2$ regions. MSE$_{min}$ was obtained as the minimum of a second order polynomial fit (black lines). The 1σ confidence interval, where MSE equals the value calculated from Eq. 5, is indicated by the horizontal lines. A) diagnostic submodel, each point represents a simulation with a different low O$_2$ ratio, B) prognostic model, "no c" is with no N$_2$O consumption i.e. net production = gross production. All other lines have a constant gross production (see legend for a description of the symbols, Tg N y^{-1}), and net production varies with different N$_2$O consumption rates. Range of parameter values is given in the supplementary material Section 8.7.

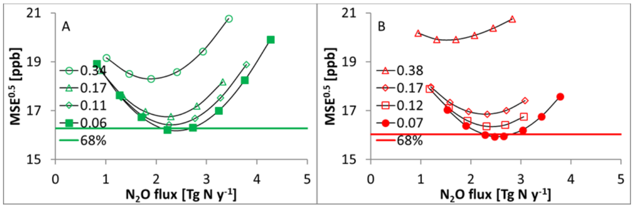

Figure 10. MSE$^{0.5}$ for the two N$_2$O submodels compared to the ΔpN$_2$O database as a function of global N$_2$O flux at different (net) N$_2$O production rates in the low O$_2$ regions. MSE$_{min}$ and confidence intervals as in Fig. 8. A) diagnostic submodel, the four lines represent the four best low O$_2$ production rates from Fig. 9A, each point represents a simulation, different symbols indicate different low O$_2$ ratios, points with the same symbols have different oxic N$_2$O production ratios. B) prognostic submodel, the four lines represent the optimised net production rates at the four best gross production rates from Fig 9B, points with the same symbols have different N$_2$O ratios for nitrification.

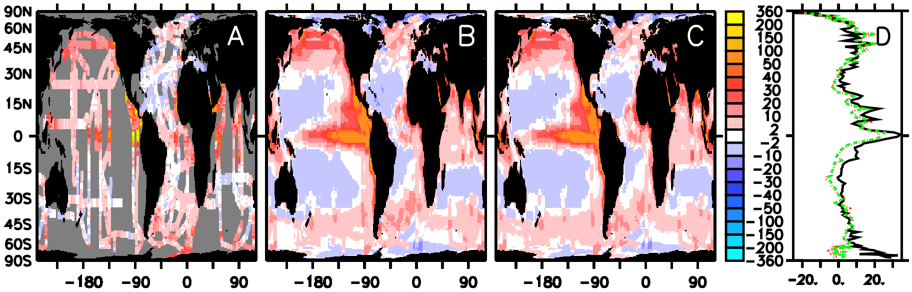

Figure 11. Surface ΔpN$_2$O (ppb). A) observations (symbol size is $5 \times 5°$), B) optimised diagnostic model, C) optimised prognostic model. Model results are for the same months where there are observations, and annual averages everywhere else. D) zonal average, Black line: observations, Green dashed: diagnostic model, Red dotted: prognostic model. Model results are for the same months and longitudes as the observations. Latitude y-axis to the left of panel A.

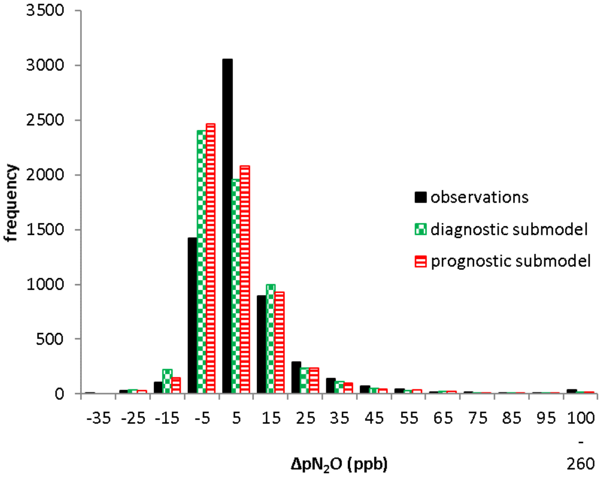

Figure 12. Frequency distribution of ΔpN_2O in the observations (solid black), and the optimised simulations of the diagnostic submodel (green squares) and the prognostic submodel (red lines).